Smooth elastic contact of cylinders by caustics: the contact length in the Brazilian disc test

S. K. KOURKOULIS, CH. F. MARKIDES, G. BAKALIS

Laboratory for Testing and Materials
Department of Mechanics
School of Applied Mathematical and Physical Sciences
National Technical University of Athens
5 Heroes of Polytechnion Avenue
Theocaris Bld., Zografou Campus, 157 73 Athens, Greece
e-mail: stakkour@central.ntua.gr

THE SMOOTH CONTACT OF TWO ELASTIC CYLINDERS compressed against each other along a common generatrix is studied analytically and experimentally. The main objective is the quantification of the length of the contact arc. For the analytic study, the complex potentials method is employed while experimentally the contact arc's length is determined by extending the reflected caustics technique. A series of experiments are then carried out using the device suggested by the International Society for Rock Mechanics for the standardized implementation of the Brazilian test and the typical set-up of the reflected caustics method. The experimental results are compared to the analytically determined ones. The agreement is satisfactory especially for low load levels, ensuring validity of the linear elasticity assumption.

Key words: reflected caustics, elastic contact, Brazilian disc test, contact arc, complex potentials.

1. Introduction

THE COMPRESSION OF A DISC-SHAPED SPECIMEN between the cylindrical jaws of the device suggested by the International Society for Rock Mechanics (ISRM) for the standardized execution of the Brazilian disc test is a typical contact problem of two elastic cylindrical bodies. However, it is rarely studied as a contact problem since it is considered that the stress field at the disc's center (which is supposed to be directly related to the tensile strength of the specimen's material [1]) is more or less insensitive to the exact conditions prevailing in the immediate vicinity of the load application area [2]. In this context, it is usually assumed that contact is realized along a "small" arc of arbitrarily predefined length, equal to a few degrees, while loading is simulated by either a point load [3] or uniformly distributed radial pressure [1]. Nevertheless, recent studies pointed out that, in spite of the above insensitivity, the contact conditions strongly in-

fluence the local stress field around the contact arc which, in turn, may lead to premature failure undermining the validity of the test results [4, 5].

In this context, the standardized Brazilian disc test configuration was recently studied analytically as a contact problem [6]. Interesting conclusions were drawn about the contact arc's length and its dependence on the external load and also about the distribution of pressure along the contact arc and its influence on the stress field. The above results were experimentally assessed by the digital image correlation (DIC) technique and the agreement was satisfactory [7]. However, the experimental data in the specific study were obtained from the $0 < r/R_1 < 0.95$ portion of the disc (R_1 is the disc's radius) since as $r/R_1 \to 1$ the accuracy of the DIC technique is downgraded by optical effects due to the geometric discontinuity at $r = R_1$ (the disc is thinner than the jaws). On the other hand, the equipment required for the laboratory application of the DIC technique is expensive, while its use for practical purposes is rather complicated and time-consuming. In order to minimize the above drawbacks the experimental technique of caustics is employed here aiming to: (i) a more accurate experimental determination of the contact arc's length by drawing data directly from the contact area and (ii) the standardization of a relatively simple easy-to-use experimental procedure.

The optical method of caustics is a powerful technique highly sensitive to stress gradients, while the equipment required for its application consists of a simple He-Ne laser and two lenses. It was Manogg [8–11] who introduced the method of transmitted caustics in 1964, while a few years later Theocaris [12, 13] introduced the method of reflected caustics. Since its introduction the method of caustics was used by many researchers, as it is described analytically by Kalthoff [14] in his concise review paper. Nowadays, the application field of the method covers a wide variety of problems ranging from the intensity of stress fields [15, 16], to dynamic loading conditions [17–23] and plasticity problems [24]. It has been used also for determining the J-integral [25], the stress-optical constants [26] and the crack-tip position [27]. Both traditional and novel materials are studied using either reflected or transmitted caustics including birefringent- [28], anisotropic- [29–32], rock-like [33], and even graded-materials [34]. Moreover, Younis [35] proposed recently an experiment based on the method of saustics for educational purposes. The use of caustics for the solution of contact problems dates back to 1978 [36, 37] and since then it has been uninterruptedly continued [38, 39].

The method of reflected caustics, employed in the present study, is based on simple principles of geometric optics, as described in Subsection 2.2. The underlying principle is that if a light beam (of either parallel, convergent or divergent rays) impinges on a specimen at the vicinity of an intense stress field, the reflected rays received on a reference plane (parallel to the plane of the specimen)

will concentrate along a strongly illuminated curve, the caustic, due to the specimen's strong thickness variations resulting from the local intensity of the stress field. The shape and dimensions of this illuminated locus permit quantitative investigation of critical features of the stress field and of the geometry of the deformed area. It is the latter property that will be used in the present study to determine the contact length developed during the compression of disc-shaped specimens between the jaws of the ISRM device.

In this manner, the method is here properly adapted for the case of two elastic cylinders in contact and next it is applied for the study of the Brazilian disc test given that the specific configuration closely resembles that of two cylinders in contact along a common generatix pressed against each other. In order to improve the accuracy of the results the traditional approach for the derivation of the caustics' formulae is here optimized by taking into account the actual shape of the "initial curve", i.e., the geometric locus of the disc's points which under specific conditions [12] provide the set of reflected rays forming the caustic curve. The "initial curve" depends on the optical constants of the material, the type of light bundle impinging on the plate (parallel, converging or diverging light rays), the optical arrangement and the inclination of the rays with respect to the plate. According to the classic literature the "initial curve" is described in terms of the undeformed configuration [12], while, on the contrary, the respective equations are re-derived in the present study with respect to the deformed state.

The improved formulae obtained are applied for the determination of the contact length between the disc and jaw in the familiar ISRM apparatus and the results obtained are compared to the ones given by the analytic solution [6] which is very shortly outlined in Section 2.1 for the sake of completeness of the paper. As it will be shown, the results are satisfactory as long as the elastic linearity assumption is valid.

2. Theoretical considerations

2.1. The disc and jaw as cylinders in contact: the contact length by complex analysis [6]

The ISRM apparatus for the standardized Brazilian disc test (Fig. 1a) consists of two jaws, the inner surface of which is cylindrical of radius $R_2 = 1.5R_1$. As the jaws are smoothly compressed against the disc by a force $P_0 = P_{\mathrm{frame}}/t$ (t is the disc thickness) contact is realized along a finite area which, if projected on the plane normal to the axial lines, forms an arc of length 2ℓ. The length of this arc and the respective contact stresses were recently obtained [6] using complex potentials [40]. The disc (S_1) and jaw (S_2) are considered in the $z = x + iy = re^{i\vartheta}$ plane (Fig. 1b). The parts of their boundaries that will come in
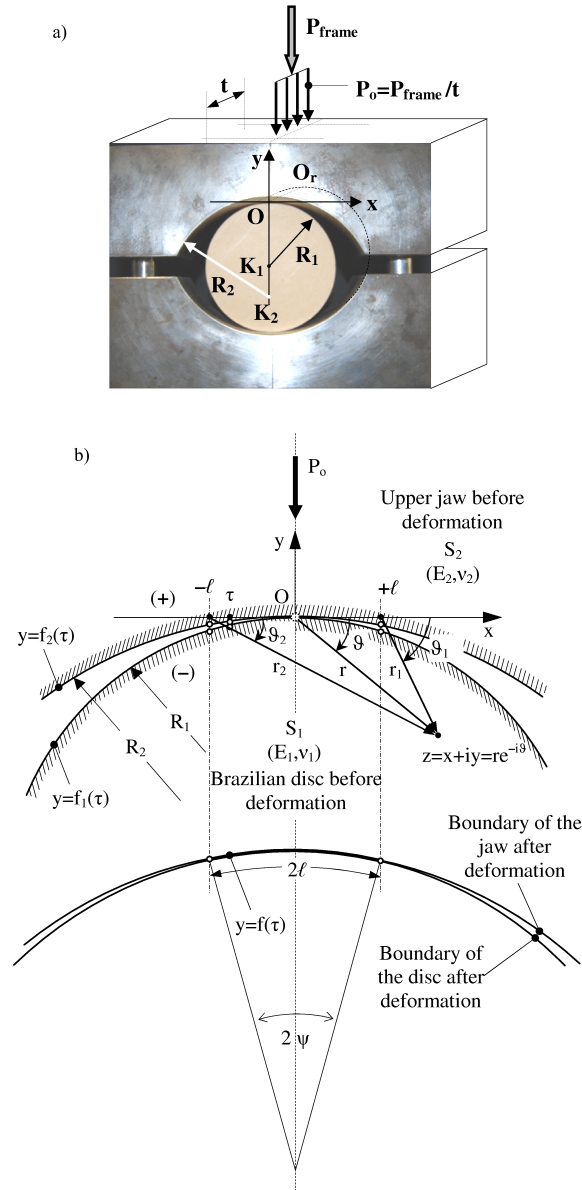
Fig. 1. a) The device suggested by ISRM for the standardized implementation of the Brazilian disc test, b) the mathematical problem and the definition of symbols.

contact are denoted by $(-\ell, +\ell)$. The reference system's origin is the mid-point O of $(-\ell, +\ell)$. Since 2ℓ is very small, the disc and jaw are approximated as half-planes and $(-\ell, +\ell)$ lies on x-axis. Any point z within $-\ell, +\ell$ is denoted by τ. The complex potentials $\Phi_j(z)$, $j = 1, 2$ characterizing elastic equilibrium of S_j,

are analytically continued to the entire plane (through the unloaded boundary parts of S_j) becoming sectionally holomorphic functions with $(-\ell, +\ell)$ being their common discontinuity line. It holds [40]:

$$(2.1) \qquad \sigma_{yy_j} - i\sigma_{xy_j} = \Phi_j(z) - \Phi_j(\overline{z}) + (z - \overline{z})\overline{\Phi'_j}(\overline{z}),$$

$$(2.2) \qquad 2\mu_j(u'_j + iv'_j) = \kappa_j\Phi_j(z) + \Phi_j(\overline{z}) - (z - \overline{z})\overline{\Phi'_j}(\overline{z}),$$

$$(2.3) \qquad 2\mu_j(u_j + iv_j) = \kappa_j\varphi_j(z) + \varphi_j(\overline{z}) - (z - \overline{z})\overline{\varphi'_j}(\overline{z}) + C, \qquad j = 1, 2,$$

C corresponds to rigid body displacements. Moreover, $\varphi'_j(z) = \Phi_j(z)$, $\kappa_j = (3 - \nu_j)/(1 + \nu_j)$ for plane stress or $\kappa_j = 3 - 4\nu_j$ for plane strain and $\mu_j = E_j/[2(1 + \nu_j)]$. E_j and ν_j are Young's moduli and Poisson's ratios, respectively. Over-bar denotes conjugate complex value and prime first-order derivative. For the specific problem, the boundary conditions are

$$(2.4) \qquad \begin{aligned} \sigma_{xy_j}^{\mp} &= 0, \quad \text{on the entire } x\text{-axis,} \\ \sigma_{yy_j}^{\mp} &= 0, \quad \text{on } x\text{-axis except } (-\ell, +\ell) \\ \sigma_{yy_j}^{\mp} &= -P(\tau), \quad \text{along } (-\ell, +\ell), \, j = 1, 2, \end{aligned}$$

$$(2.5) \qquad v_1^{-\prime} - v_2^{+\prime} = f'(\tau), \quad \text{on } (-\ell, +\ell).$$

$P(\tau) > 0$ denotes the normal stresses and $f(\tau) = f_1(\tau) - f_2(\tau)$ ($y = f_1(\tau)$, $y = f_2(\tau)$ are the boundaries of S_j before deformation). Superscripts $(-)$, $(+)$ refer to values for z tending to τ on $(-\ell, +\ell)$ from the lower and upper half-planes, respectively. For $j = 1, 2$ and τ on $(-\ell, +\ell)$ Eqs. (2.1) yield:

$$(2.6) \quad -\sigma_{yy_1}^{-} = P(\tau) = \Phi_1^{+}(\tau) - \Phi_1^{-}(\tau) \quad \text{and} \quad -\sigma_{yy_2}^{+} = P(\tau) = \Phi_2^{-}(\tau) - \Phi_2^{+}(\tau).$$

Hence, $\Phi_1(z) + \Phi_2(z)$ is holomorphic in the entire plane and assuming it vanishes at infinity $\Phi_2(z) = -\Phi_1(z)$. On the other hand, Eqs. (2.2) for $j = 1$ and τ on $(-\ell, +\ell)$ yields

$$(2.7) \qquad 2\mu_1(u_1^{-\prime} + iv_1^{-\prime}) = \kappa_1\Phi_1^{-}(\tau) + \Phi_1^{+}(\tau),$$

$$(2.8) \qquad 2\mu_1(u_1^{-\prime} - iv_1^{-\prime}) = \kappa_1\overline{\Phi_1^{-}}(\tau) + \overline{\Phi_1^{+}}(\tau).$$

For smooth contact and $\Phi_1(z)$ vanishing at infinity $\overline{\Phi_1}(z) = -\Phi_1(z)$. Then Eq. (2.8) becomes:

$$(2.9) \qquad 2\mu_1(u_1^{-\prime} - iv_1^{-\prime}) = -\kappa_1\Phi_1^{+}(\tau) - \Phi_1^{-}(\tau).$$

By subtracting Eq. (2.9) from Eq. (2.7) the following is obtained:

$$(2.10) \qquad iv_1^{-\prime} = \frac{\kappa_1 + 1}{4\mu_1}[\Phi_1^{+}(\tau) + \Phi_1^{-}(\tau)].$$

Adding Eq. (2.10) to the one similarly obtained for the jaw it is found using Eq. (2.5) that

(2.11) $\Phi_1^+(\tau) + \Phi_1^-(\tau) = if'(\tau)/K$ with $K = (\kappa_1 + 1)/4\mu_1 + (\kappa_2 + 1)/4\mu_2.$

Considering function $\sqrt{\ell^2 - z^2} = -iX(z)$, the solution of Eq. (2.11) reads as

$$(2.12) \qquad \Phi_1(z) = \frac{1}{2\pi K\sqrt{\ell^2 - z^2}} \int\limits_{-\ell}^{+\ell} \frac{f'(\tau)\sqrt{\ell^2 - \tau^2}d\tau}{\tau - z} + \frac{P_0}{2\pi\sqrt{\ell^2 - z^2}}.$$

Introducing Eq. (2.12) into the first of Eqs. (2.6) and using Plemelj formulae the pressure distribution at any point $\tau_0 \in [-\ell, +\ell]$ becomes

$$(2.13) \qquad P(\tau_0) = \frac{1}{\pi K\sqrt{\ell^2 - \tau_0^2}} \int\limits_{-\ell}^{+\ell} \frac{f'(\tau)\sqrt{\ell^2 - \tau^2}d\tau}{\tau - \tau_0} + \frac{P_0}{\pi\sqrt{\ell^2 - \tau_0^2}}.$$

Demanding that $P(\tau)$ must remain bounded at points $\pm\ell$ [40] it can be written:

$$\Phi_1(z) = \frac{\sqrt{\ell^2 - z^2}}{2\pi K} \int\limits_{-\ell}^{+\ell} \frac{f'(\tau)d\tau}{\sqrt{\ell^2 - \tau^2}(\tau - z)},$$

(2.14)

$$P(\tau_0) = \frac{\sqrt{\ell^2 - \tau_0^2}}{\pi K} \int\limits_{-\ell}^{+\ell} \frac{f'(\tau)d\tau}{\sqrt{\ell^2 - \tau^2}(\tau - \tau_0)},$$

$$(2.15) \qquad \int\limits_{-\ell}^{+\ell} \frac{f'(\tau)d\tau}{\sqrt{\ell^2 - \tau^2}} = 0, \qquad \int\limits_{-\ell}^{+\ell} \frac{f'(\tau)\tau d\tau}{\sqrt{\ell^2 - \tau^2}} = KP_0.$$

Assuming that $f_j(\tau) = -(\tau^2/2R_j)$, i.e., the boundaries of the two circular bodies approximate along $(-\ell, +\ell)$ two parabolas of the same curvature at the vertex point O, Eqs. (2.14) and (2.15) yield:

$$\Phi_1(z) = \frac{1}{6R_1 K}(\sqrt{\ell^2 - z^2} + iz),$$

(2.16)

$$P(\tau) = \frac{1}{3R_1 K}\sqrt{\ell^2 - \tau^2},$$

$$\ell = \sqrt{\frac{6R_1 K P_0}{\pi}}.$$

2.2. The disc-jaw contact length by the reflected caustics method

2.2.1. Adopting the classic approach. A parallel light beam impinges normally on a disc in equilibrium under the action of the force P_{frame} (Fig. 2a). Reflected light rays are received on a screen parallel to the disc at a distance Z_0. In case light is reflected from the points P with severe lateral deformation, a strongly
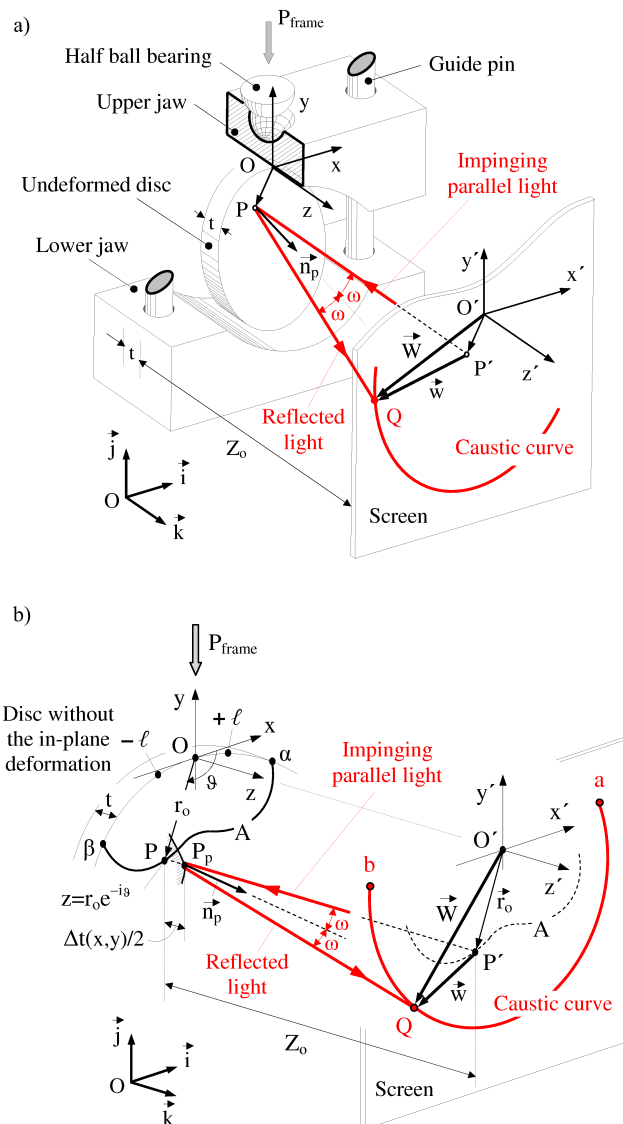

FIG. 2. a) The principles of the reflected caustics method, b) the formation of the reflected caustic curve according to the traditional approach.

illuminated locus of points Q, the caustic, is formed on the screen. A Cartesian reference system $\{O; x, y, z\}$ is considered at the apex O and a second one $\{O'; x', y', z'\}$ (obtained from $\{O; x, y, z\}$ by simple translation equal to Z_0) is considered on the screen. If P' is the projection of P on the screen, then the caustic is described by the vector:

$$(2.17) \qquad \overrightarrow{W} = \overrightarrow{O'P'} + \overrightarrow{w}.$$

$|\overrightarrow{O'P'}| = |\overrightarrow{OP}|$ and $\overrightarrow{w}$ define the deviation of light at P. According to Snell's law this deviation corresponds to an angle 2ω where ω is the angle subtended by the incident light ray and the normal $\overrightarrow{n_p}$ to the distorted surface at P. For small angles of deflection ω it holds:

$$(2.18) \qquad \overrightarrow{w} = Z_0 \overrightarrow{\nabla} \left[\Delta t\left(x, y\right) \right] = Z_0 \overrightarrow{\nabla} \left[\frac{\nu_1 t}{E_1} \left(\sigma_1 + \sigma_2\right) \right],$$

where $\Delta t(x,y)$ is the thickness change due to Poisson's effects and

$$\overrightarrow{\nabla} = \frac{\partial}{\partial x} \overrightarrow{i} + \frac{\partial}{\partial y} \overrightarrow{j}.$$

Assume now that the in-plane undeformed disc's front face lies in the complex plane $z = x + iy = re^{-i\vartheta}$, $\vartheta \in [0, \pi]$ (Fig. 2b). The origin of the Cartesian reference is again (as in Fig. 2a) at the apex O and now the complex variable z should not be confused with the z-coordinate axis. Let the points P, providing the caustic curve, correspond to points $z = r_0 e^{-i\vartheta}$ (the subscript at r_0 distinguishes the specific points from any other arbitrary point z on the disc). In Fig. 2b, the translation of P (or $z = r_0 e^{-i\vartheta}$) to P_p due to the $\Delta t(x, y)/2$ change of thickness is also shown. According to the classic approach, the points P, which refer to the in-plane undeformed disc, belong to the "initial curve" denoted in the figure by A. Introducing in Eq. (2.18) the familiar formula [40]:

$$(2.19) \qquad \sigma_1 + \sigma_2 = 4\Re\Phi_1(z),$$

$\Re$ is the real part and introducing also the magnification factor of the set-up $\lambda_m = (Z_0 \pm Z_i)/Z_i$ (+/− for divergent/convergent light beams, respectively, and Z_i the distance of the focus of the respective light bundle from the front face of the disc), Eq. (2.17) is written in complex form as

$$(2.20) \qquad W = \lambda_m z + \underbrace{4Z_0 t \overbrace{\frac{\nu}{E}}^{c_f}}_{C} \overline{\Phi_1'(z)} = \lambda_m z + C\overline{\Phi_1'(z)}.$$

Separating in Eq. (2.20) real from imaginary $\Im$ parts, the caustic is written in parametric form as

$$(2.21) \qquad W_{x'} = \lambda_m x + C\Re\{\overline{\Phi_1'(z)}\}, \qquad W_{y'} = \lambda_m y + C\Im\{\overline{\Phi_1'(z)}\}.$$

Zeroing the Jacobian determinant of the above transformation leads to

$$(2.22) \qquad C\left|\frac{\Phi_1''(z)}{\lambda_m}\right| = 1$$

(double prime denotes second order derivative) which represents the "initial curve". Substituting $\Phi_1(z)$ from Eqs. (2.16) into Eq. (2.22) and introducing the complex variables $z_1 = z - \ell = r_1 e^{-i\vartheta_1}$ and $z_2 = z + \ell = r_2 e^{-i\vartheta_2}$ $(\vartheta_1, \vartheta_2 \in [0, \pi])$ (Fig. 1b), one obtains

$$(2.23) \qquad r_1 r_2 = \left(2 \cdot \underbrace{\frac{C}{12|\lambda_m|KR_1}}_{C^*}\right)^{\frac{2}{3}} \ell^{\frac{4}{3}} = (2|C^*|)^{\frac{2}{3}} \ell^{\frac{4}{3}}.$$

In addition, it holds that $r_{1,2} = \sqrt{r_0^2 + \ell^2 \mp 2r_0\ell\cos\vartheta}$ (Fig. 1b) and therefore Eq. (2.23) yields

$$(2.24) \qquad r_0^4 - 2r_0^2\ell^2\cos 2\vartheta + \ell^4 - (2|C^*|\ell^2)^{\frac{4}{3}} = 0.$$

Hence, for $2|C^*| \geq \ell$ the radius of the "initial curve" reads as

$$(2.25) \qquad r_0 = \ell\sqrt{\cos 2\vartheta + \sqrt{\cos^2 2\vartheta - 1 + (2|C^*|/\ell)^{\frac{4}{3}}}}.$$

In addition, Eqs. (2.21) provide the classic parametric equations of the caustic as

$$(2.26)$$
$$W_{x'} = \lambda_m\left[r_0\cos\vartheta - r_0\left(\frac{2|C^*|}{\ell}\right)^{\frac{2}{3}}\sin\left(\vartheta - \frac{\vartheta_1 + \vartheta_2}{2}\right)\right],$$
$$W_{y'} = \lambda_m\left[-r_0\sin\vartheta - 2C^* + r_0\left(\frac{2|C^*|}{\ell}\right)^{\frac{2}{3}}\cos\left(\vartheta - \frac{\vartheta_1 + \vartheta_2}{2}\right)\right].$$

The "initial curve" and the respective caustic according to Eqs. (2.25) and (2.26) are plotted in Fig. 3 for a relatively low external load level (as it will be shown later for high loads or equivalently for long contact arcs, the "initial curve" tends to split into two independent curves). For plotting Fig. 3, plane stress conditions were assumed for a disc made of PMMA (elastic modulus $E_p = 3.2$ GPa, Poisson's ratio $\nu_p = 0.38$ and yield stress equal to about $\sigma_y = 28$ MPa)
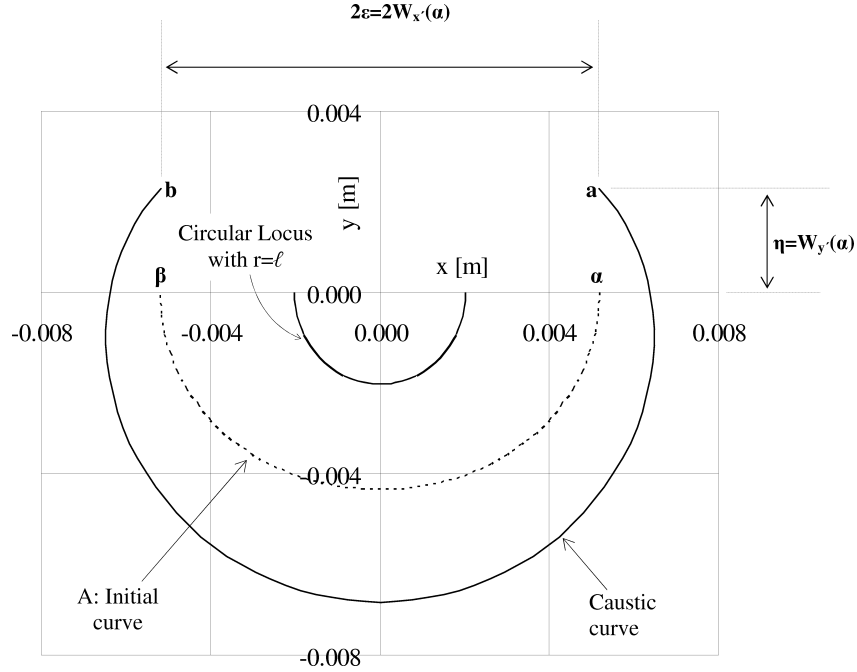
FIG. 3. The "initial curve" and the respective caustic due to the disc-jaw contact for a relatively low load level according to the traditional approach.

and steel jaws ($E_s = 210$ GPa and $\nu_s = 0.30$). The diameter of disc was $D = 100$ mm and its thickness (length) was $t = 10$ mm. An overall external load equal $P_{\text{frame}} = 30$ kN was assumed creating at the disc's center a stress equal to about 19 MPa, well below the yield stress. λ_m was set equal to 2. It is seen from Fig. 3 that the "radius" of the "initial curve" is more than two times the contact semi-length while for the specific load the caustic is of almost cyclic shape.

For $\{\vartheta, \vartheta_1, \vartheta_2\} = 0, \pi$ the coordinates (x_α, y_α), (x_β, y_β) and (x'_a, y'_a), (x'_b, y'_b) of the end-points, (α, β) and (a, b) of the "initial curve" and the caustic, respectively (Figs. 2b and 3), are given as

$$(2.27) \qquad \left.\begin{array}{c} x_\alpha \\ x_\beta \end{array}\right\} = \pm r_0(\alpha) = \pm \ell \sqrt{1 + \left(\frac{2|C^*|}{\ell}\right)^{2/3}}, \qquad y_\alpha = y_\beta = 0,$$

$$(2.28) \qquad x'_a = W_{x'}(\alpha) = -x'_b = -W_{x'}(\beta) = \lambda_m r_0(\alpha),$$

$$(2.29) \qquad y'_a = W_{y'}(\alpha) = y'_b = W_{y'}(\beta) = \lambda_m \left[r_0(\alpha)\left(\frac{2|C^*|}{\ell}\right)^{2/3} - 2C^* \right].$$

Combination of Eqs. (2.27)–(2.29) yields the contact length ℓ, in terms of the distance $2\varepsilon = (ab) = 2W_{x'}(\alpha)$ or of the elevation $\eta = W_{y'}(\alpha) = W_{y'}(\beta)$ of points a and b, respectively, as

(2.30) $$\ell^2 + 2|C^*|^{2/3}\ell^{4/3} - \frac{[2W_{x'}(\alpha)]^4}{4\lambda_m^2} = 0,$$

(2.31) $$\ell = 2C^*\left[\left(\frac{W_{y'}(\alpha)}{2|C^*|\lambda_m} + 1\right)^2 - 1\right]^{3/2}.$$

In other words, by employing the method of caustics the contact length can be determined in terms of quantities experimentally measurable. Although Eq. (2.31) is simpler than Eq. (2.30), it is rarely used in practice since it is difficult to determine experimentally the $y' = 0$ line.

2.2.2. An improved approach. The main limitation of the analysis in Subsection 2.2.1 is that the components of the displacement field were assumed negligibly small in comparison to the "initial curve" itself. As a result, the size and shape of the "initial curve" were determined ignoring disc's in-plane deformation. Although such an assumption is quite acceptable for discs made of brittle materials it could lead to erroneous results in case the disc is made of materials of reduced brittleness.

In this direction, the problem of determining the contact length by caustics is reconsidered according to an improved procedure taking into account the components of the displacement field. Consider the in-plane deformed front face of the disc in the $z = x + iy = re^{-i\vartheta}$, $\vartheta \in [0, \pi]$ complex plane (Fig. 4). Omitting rigid body displacements, a Cartesian reference $\{O; x, y, z\}$ is attached to the in-plane deformed disc at the apex O. In addition, as in Subsection 2.2.1, another reference system $\{O'; x', y', z'\}$ obtained from $\{O; x, y, z\}$ by simple translation equal to Z_0 is considered on the screen. Therefore, the transformation considered previously between the in-plane undeformed disc and the screen will be realized now between the in-plane deformed disc and the screen. According to this line of thought, the locus of points, A of the undeformed disc (drawn with thin line in Fig. 4) does not any longer represent the "initial curve". It rather represents a set of points P (or $z = r_0 e^{-i\vartheta}$) which *after* adding to them the in-plane displacement field $\{u, v\}$ (colored green in Fig. 4) yield the locus P_d forming the actual "initial curve" A_d. In turn, P_d shifts to P_p due to the out-of-plane deformation $\Delta t/2$. Then, impinging light is reflected on P_p and its image Q on the screen belongs to the actual caustic curve. Strictly speaking the actual "initial curve" is not a plane curve due to the out-of-plane deformation $\Delta t(x, y)/2$. However, in a first approximation (recall that $\Delta t(x, y)/2$ is too small compared to Z_0) the points

Fig. 4. The formation of the caustic curve according to the improved approach.

P_d can accurately enough stand for P_p and, accordingly, A_d can stand as the actual "initial curve".

It can be easily seen (from the zeroing of the determinant of the transformation between the in-plane deformed disc and the screen) that according to the present approach the points P providing the "initial curve" are still given approximately by Eq. (2.22) due to the assumption of small deformations adopted. However, the "initial curve" itself is more accurately described. On the other hand, the parametric equations of the caustic become

$$(2.32) \qquad \begin{aligned} W_{x'} &= \lambda_m[x + u(x,y)] + C\Re\{\overline{\Phi_1'(z)}\}, \\ W_{y'} &= \lambda_m[y + v(x,y)] + C\Im\{\overline{\Phi_1'(z)}\}. \end{aligned}$$

Eqations (2.32) differ from Eqs. (2.21) of the classic approach since now the displacement components have been included in the respective expressions. It is thus imperative to determine the displacements of points P (or $z = r_0 e^{-i\vartheta}$) providing the "initial curve". Thus, $\varphi_1(z)$ is firstly obtained by integrating $\Phi_1(z)$ from Eqs. (2.16), as follows:

$$(2.33) \qquad \varphi_1(z) = \frac{1}{12R_1K}\left(z\sqrt{\ell^2 - z^2} + \ell^2 \text{Arc} \tan\frac{z}{\sqrt{\ell^2 - z^2}} + iz^2\right).$$

Substituting $\varphi_1(z)$ into Eqs. (2.3) for $j = 1$ and taking under consideration Eq. (2.23), the displacement components of any point on the A locus are obtained as

$$(2.34) \quad u(r_0, \vartheta) = \frac{1}{24\mu R_1 K}\left\{(\kappa - 1)\left[r_0^2 \sin 2\vartheta - r_0(2|C^*|)^{\frac{1}{3}}\ell^{\frac{2}{3}}\sin\left(\vartheta + \frac{\vartheta_1 + \vartheta_2}{2}\right)\right.\right.$$

$$+ \frac{\ell^2}{2}\left(\tan^{-1}\frac{r_0 \sin\vartheta + (2|C^*|)^{\frac{1}{3}}\ell^{\frac{2}{3}}\sin\frac{\vartheta_1+\vartheta_2}{2}}{r_0 \cos\vartheta + (2|C^*|)^{\frac{1}{3}}\ell^{\frac{2}{3}}\cos\frac{\vartheta_1+\vartheta_2}{2}}\right.$$

$$\left.\left.- \tan^{-1}\frac{r_0 \sin\vartheta - (2|C^*|)^{\frac{1}{3}}\ell^{\frac{2}{3}}\sin\frac{\vartheta_1+\vartheta_2}{2}}{r_0 \cos\vartheta - (2|C^*|)^{\frac{1}{3}}\ell^{\frac{2}{3}}\cos\frac{\vartheta_1+\vartheta_2}{2}}\right)\right]$$

$$\left.+ 4r_0 \sin\vartheta\left[r_0 \cos\vartheta - (2|C^*|)^{\frac{1}{3}}\ell^{\frac{2}{3}}\cos\frac{\vartheta_1 + \vartheta_2}{2}\right]\right\},$$

$$(2.35) \quad v(r_0, \vartheta) = \frac{1}{24\mu R_1 K}\left\{(\kappa + 1)\left[r_0^2 \cos 2\vartheta - r_0(2|C^*|)^{\frac{1}{3}}\ell^{\frac{2}{3}}\cos\left(\vartheta + \frac{\vartheta_1 + \vartheta_2}{2}\right)\right.\right.$$

$$+ \frac{\ell^2}{4}\ln\frac{r_0^2 + (2|C^*|)^{\frac{2}{3}}\ell^{\frac{4}{3}} + 2r_0(2|C^*|)^{\frac{1}{3}}\ell^{\frac{2}{3}}\cos(\vartheta - \frac{\vartheta_1+\vartheta_2}{2})}{r_0^2 + (2|C^*|)^{\frac{2}{3}}\ell^{\frac{4}{3}} - 2r_0(2|C^*|)^{\frac{1}{3}}\ell^{\frac{2}{3}}\cos(\vartheta - \frac{\vartheta_1+\vartheta_2}{2})}\right]$$

$$\left.+ 4r_0 \sin\vartheta\left[r_0 \sin\vartheta - (2|C^*|)^{\frac{1}{3}}\ell^{\frac{2}{3}}\sin\frac{\vartheta_1 + \vartheta_2}{2}\right]\right\}.$$

Clearly, the coordinates of points P_d on the "initial curve" A_d are obtained by adding to the points P (or $z = r_0 e^{-i\vartheta}$; r_0 is given by Eq. (2.25)) of A, the above determined displacement field $u(r_0, \vartheta) + iv(r_0, \vartheta)$. Finally, substitution of Eqs. (2.34), (2.35) in Eqs. (2.32) gives the new improved version of Eqs. (2.26) for the parametric equations of caustics as

$$(2.36) \quad W_{x'} = \lambda_m\left[r_0 \cos\vartheta - r_0\left(\frac{2|C^*|}{\ell}\right)^{\frac{2}{3}}\sin\left(\vartheta - \frac{\vartheta_1 + \vartheta_2}{2}\right)\right]$$

$$+ \frac{\lambda_m}{24\mu R_1 K}\left\{(\kappa - 1)\left[r_0^2 \sin 2\vartheta - r_0(2|C^*|)^{\frac{1}{3}}\ell^{\frac{2}{3}}\sin\left(\vartheta + \frac{\vartheta_1 + \vartheta_2}{2}\right)\right.\right.$$

$$+ \frac{\ell^2}{2}\left(\tan^{-1}\frac{r_0 \sin\vartheta + (2|C^*|)^{\frac{1}{3}}\ell^{\frac{2}{3}}\sin\frac{\vartheta_1+\vartheta_2}{2}}{r_0 \cos\vartheta + (2|C^*|)^{\frac{1}{3}}\ell^{\frac{2}{3}}\cos\frac{\vartheta_1+\vartheta_2}{2}}\right.$$

$$\left.\left.- \tan^{-1}\frac{r_0 \sin\vartheta - (2|C^*|)^{\frac{1}{3}}\ell^{\frac{2}{3}}\sin\frac{\vartheta_1+\vartheta_2}{2}}{r_0 \cos\vartheta - (2|C^*|)^{\frac{1}{3}}\ell^{\frac{2}{3}}\cos\frac{\vartheta_1+\vartheta_2}{2}}\right)\right]$$

$$\left.+ 4r_0 \sin\vartheta\left[r_0 \cos\vartheta - (2|C^*|)^{\frac{1}{3}}\ell^{\frac{2}{3}}\cos\frac{\vartheta_1 + \vartheta_2}{2}\right]\right\},$$

$$(2.37) \quad W_{y'} = \lambda_m \left[-r_0 \sin\vartheta - 2C^* + r_0 \left(\frac{2|C^*|}{\ell}\right)^{\frac{2}{3}} \cos\left(\vartheta - \frac{\vartheta_1 + \vartheta_2}{2}\right)\right]$$

$$+ \frac{\lambda_m}{24\mu R_1 K}\left\{(\kappa+1)\left[r_0^2 \cos 2\vartheta - r_0(2|C^*|)^{\frac{1}{3}}\ell^{\frac{2}{3}} \cos\left(\vartheta + \frac{\vartheta_1 + \vartheta_2}{2}\right)\right.\right.$$

$$+ \frac{\ell^2}{4}\ell n\frac{r_0^2 + (2|C^*|)^{\frac{2}{3}}\ell^{\frac{4}{3}} + 2r_0(2|C^*|)^{\frac{1}{3}}\ell^{\frac{2}{3}}\cos(\vartheta - \frac{\vartheta_1+\vartheta_2}{2})}{r_0^2 + (2|C^*|)^{\frac{2}{3}}\ell^{\frac{4}{3}} - 2r_0 t(2|C^*|)^{\frac{1}{3}}\ell^{\frac{2}{3}}\cos(\vartheta - \frac{\vartheta_1+\vartheta_2}{2})}\right]$$

$$+ 4r_0 \sin\vartheta\left[r_0 \sin\vartheta - (2|C^*|)^{\frac{1}{3}}\ell^{\frac{2}{3}}\sin\frac{\vartheta_1+\vartheta_2}{2}\right]\Bigg\}.$$

For $\{\vartheta, \vartheta_1, \vartheta_2\} = 0, \pi$ the coordinates $(x_{\alpha_d}, y_{\alpha_d})$, $(x_{\beta_d}, y_{\beta_d})$ and (x'_{a_d}, y'_{a_d}), (x'_{b_d}, y'_{b_d}) of the end-points (α_d, β_d) and (a_d, b_d) of the "initial curve" and caustic, respectively (Figs. 4, 5 and 8), are given as

$$(2.38) \qquad \left.\begin{array}{c} x_{\alpha_d} \\ x_{\beta_d}\end{array}\right\} = \pm\ell\sqrt{1 + \left(\frac{2\,|C^*|}{\ell}\right)^{\frac{2}{3}}} = \pm r_0(\alpha),$$

$$(2.39) \qquad y_{\alpha_d} = y_{\beta_d} = \frac{\kappa+1}{24\mu R_1 K}\left[r_0^2(\alpha) - r_0(\alpha)(2|C^*|)^{\frac{1}{3}}\ell^{\frac{2}{3}}\right.$$

$$\left. + \frac{\ell^2}{2}\ell n\frac{r_0(\alpha) + (2|C^*|)^{\frac{1}{3}}\ell^{\frac{2}{3}}}{r_0(\alpha) - (2|C^*|)^{\frac{1}{3}}\ell^{\frac{2}{3}}}\right],$$

$$(2.40) \quad x'_{a_d} = W_{x'}(\alpha_d) = -x'_{b_d} = -W_{x'}(\beta_d) = \lambda_m r_0(\alpha),$$

$$(2.41) \quad y'_{a_d} = W_{y'}(\alpha_d) = y'_{b_d} = W_{y'}(\beta_d)$$

$$= \lambda_m\left\{r_0(\alpha)\left(\frac{2|C^*|}{\ell}\right)^{\frac{2}{3}} - 2C^* + \frac{\kappa+1}{24\mu R_1 K}\left[r_0^2(\alpha) - r_0(\alpha)(2|C^*|)^{\frac{1}{3}}\ell^{\frac{2}{3}}\right.\right.$$

$$\left.\left. + \frac{\ell^2}{2}\ell n\frac{r_0(\alpha) + (2|C^*|)^{\frac{1}{3}}\ell^{\frac{2}{3}}}{r_0(\alpha) - (2|C^*|)^{\frac{1}{3}}\ell^{\frac{2}{3}}}\right]\right\}.$$

Notice that Eq. (2.38) and Eq. (2.40), providing the distance between the end-points of the "initial"- and the caustic-curves, are identical to the respective expressions Eqs. (2.27) and (2.28) of the classic approach. This should be expected since in the case of the Brazilian disc analyzed here it holds that $u(r_0, \vartheta = 0) = u(\alpha) = 0 = u(r_0, \vartheta = \pi) = u(\beta)$, i.e., because points α and β (of A) yielding the actual "initial curve" A_d remain stationary along the x_d-direction.

Combination of Eqs. (2.38)–(2.41) yields the contact length ℓ, in terms of the distance $2\varepsilon = (a_d b_d) = 2W_{x'}(\alpha_d)$ between points a_d and b_d, and of the elevation $\eta = W_{y'}(\alpha_d) = W_{y'}(\beta_d)$ of points a_d and b_d, respectively, through the relations

$$(2.42) \qquad \ell^2 + 2|C^*|^{\frac{2}{3}}\ell^{\frac{4}{3}} - \frac{[2W_{x'}(\alpha_d)]^4}{4\lambda_m^2} = 0,$$

$$(2.43) \qquad W_{y'}(\alpha_d) = \lambda_m \bigg\{ \ell\sqrt{1 + (2|C^*|/\ell)^{\frac{2}{3}}}(2|C^*|/\ell)^{\frac{2}{3}} - 2C^*$$

$$+ \frac{\kappa+1}{24\mu R_1 K}\bigg[\ell^2\bigg(1 + (2|C^*|/\ell)^{\frac{2}{3}}\bigg)$$

$$- \ell\sqrt{1 + (2|C^*|/\ell)^{\frac{2}{3}}}(2|C^*|)^{\frac{1}{3}}\ell^{\frac{2}{3}}$$

$$+ \frac{\ell^2}{2}\ell n\frac{\ell\sqrt{1 + (2|C^*|/\ell)^{\frac{2}{3}}} + (2|C^*|)^{\frac{1}{3}}\ell^{\frac{2}{3}}}{\ell\sqrt{1 + (2|C^*|/\ell)^{\frac{2}{3}}} - (2|C^*|)^{\frac{1}{3}}\ell^{\frac{2}{3}}}\bigg]\bigg\}.$$

Equation (2.42) is identical to Eq. (2.30). Since $2\varepsilon = (a_d b_d) = 2W_{x'}(\alpha_d)$ or $\eta = W_{y'}(\alpha_d)$ are directly measured from the caustic curve, the above relations, if solved numerically, provide the contact length ℓ. Again for practical reasons Eq. (2.42) is the one used mainly.

The improved approach introduced here is compared to the classic one in Fig. 5 where both the "initial curve" and the respective caustic as obtained by the two approaches are plotted for a PMMA disc ($D = 100$ mm, $t = 10$ mm) compressed between the steel jaws of the ISRM suggested device. The material properties and the magnification factor are those mentioned in Subsection 2.2.1. The externally applied load is now equal to 40 kN generating at the disc's center a tensile stress equal to about 25 MPa, again below the yield stress of PMMA. It is recalled here that for low load levels the "initial curve" according to the classic approach is of cyclic shape (see Fig. 3) while according to the present approach it is of elliptic shape (due to the type of the displacements added). However, for increased load levels the initial curve for both the classic and the improved approaches is depressed and tends to split into two symmetric parts, as it is seen in Fig. 5. From the same figure it is seen that the contact length is again well comparable to the characteristic dimension of the "initial curve".

On the other hand, the difference δ in the elevations η as obtained by the two approaches exceeds well 15% and the difference when calculating the contact length using Eq. (2.31) and Eq. (2.43) is of the same order. It is recalled here that $W_{x'}(\alpha)$ remains uninfluenced as already explained.
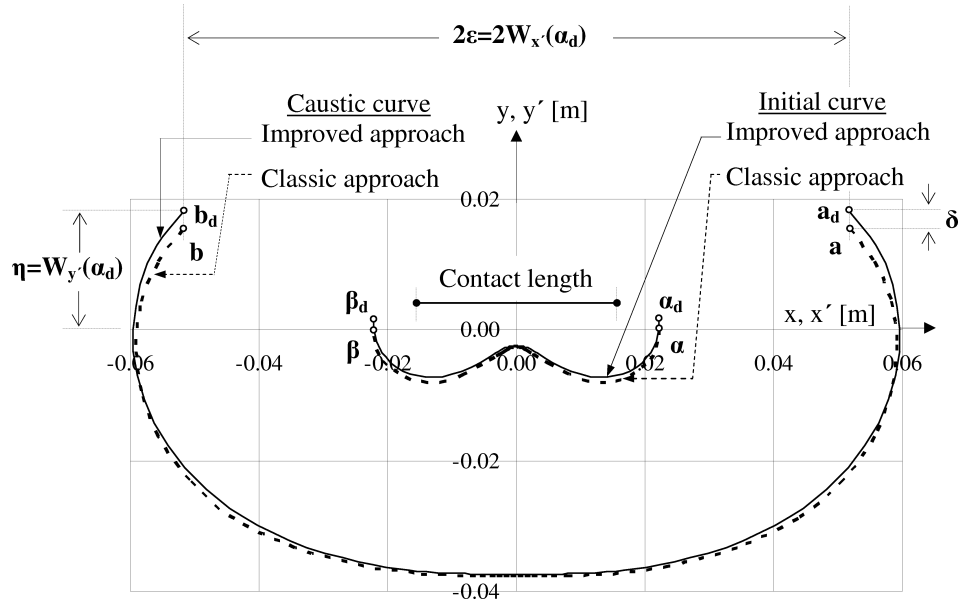
Fig. 5. Comparison of the caustic curves according to the traditional and the improved approach.

3. Experimental procedure and results

3.1. The experimental arrangement

The experimental set-up consisted of a He-Ne laser and two collimating lenses as it is shown schematically in Fig. 6. Lens L_1 transformed the diverging beam emitted from the laser to a collimated one. A second lens L_2 transformed the collimated beam into a converging one with its focal point in front of the specimen in order to better control the magnification factor λ_m of the set-up. The beam impinges on the loaded specimen and the reflected rays are driven with the aid of a semi-reflector, placed at an angle equal to 45° with respect to the specimen's plane, towards a screen forming the caustic curve. The use of the semi-reflector greatly improves the quality of the experimental results since optimum placement of the screen and normal incidence of the rays on the disc [41] are achieved (recall that using the semi-reflector the distance Z_0 becomes the sum of the specimen-semi-reflector and the semi-reflector-screen distances). The caustic curve formed on the screen was photographed at predefined load intervals. The critical quantities of the caustic curves were then measured from these photos with the aid of a standard optical arrangement and suitable commercial software.
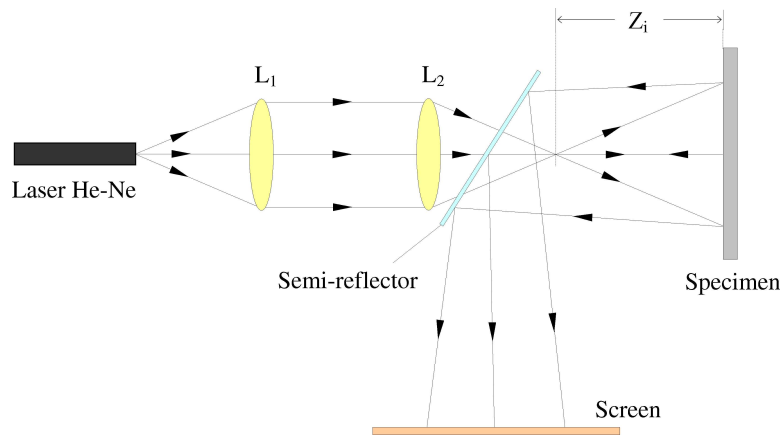
Fig. 6. Schematic representation of the experimental set-up.

3.2. The material and the specimens

The specimens of the experimental protocol were cylindrical discs of diameter $D = 100$ mm and length (thickness) $t = 10$ mm. They were cut from the same PMMA plate to avoid any variability of their mechanical properties. The choice of PMMA was based on the fact that its mechanical behaviour approaches in a satisfactory manner that of a linear elastic material (at least for stress levels not approaching the failure stress) fulfilling the main assumption adopted during the development of the caustics theory. The values of the mechanical constants adopted were $E_P = 3.2$ GPa for the modulus of elasticity and $\nu_P = 0.38$ for Poisson's ratio. The yield stress and the tensile strength were equal to about 28 MPa and 38 MPa, respectively [42]. The optical constant c_f, required for the application of the reflected caustics formula, was calculated equal to $c_f = \nu_P/E_P = 1.18 \times 10^{-10}$ m^2/N.

Special attention was given to the lateral surfaces to be as smooth as possible. The specimens were placed within the jaws of the apparatus standardized by ISRM for the implementation of the Brazilian disc test. The apparatus was mounted on an electromechanical INSTRON 1125 loading frame of capacity 50 kN. The upper jaw of the apparatus was compressed by the movable traverse of the frame against the specimen under a displacement-control loading mode at a rate equal to 0.1 mm/min. A semi-spherical head interposed between the upper jaw and the moving traverse of the frame ensured further normality of the load axis versus the upper jaw. The resulting compressive force was measured using a 50 kN load cell calibrated with a verified Wykeham Farrance compression ring of sensitivity 10.62 N. The response of the cell was linear throughout the whole load range of interest and the deviation was lower than 0.2%. The displacement

rate was calibrated also using a verified high-magnification micrometric calibrator. Again, the response was linear and the deviation did not exceed 0.4%.

3.3. Experimental results

A series of photos showing the caustic curves, at various load levels, as obtained from two typical experiments are shown in Fig. 7. It is emphasized that due to the transparency of the specimen's material two caustics are inevitably formed on the screen: one from the optical rays reflected on the front face of the specimen (the continuous external bright curve of Fig. 7) and one from the rays reflected on the rear face (the bright curve encompassed in the

Caustic from reflection on the front face

Caustic from reflection on the rear face
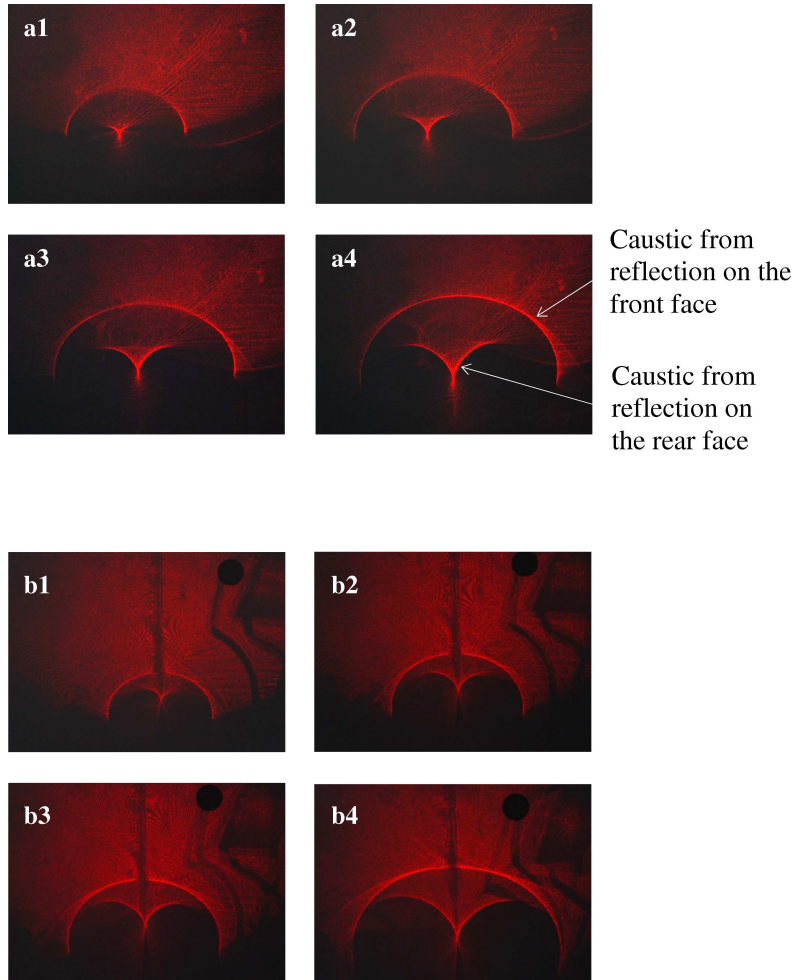
Fig. 7. The caustics for two typical tests at load levels equal to 3 (a1, b1), 6 (a2, b2), 9 (a3, b3) and 12 (a4, b4) kN.

previous one). For the purpose of the present study, only the caustic formed from the rays reflected on the front face of the disc was considered since it has the advantage to be determined with the aid of a single stress-optical constant which is moreover directly obtained from the mechanical properties of the disc's material.

According to the analysis in Subsection 2.2.2 measuring the distance $2\varepsilon = 2W_{x'}(\alpha_d)$ between the extreme points a_d and b_d of the caustic curves from reflection on the front face of the specimens (Fig. 8, embedded photo), one obtains directly the contact length by solving numerically Eq. (2.42). The reason for choosing the quantity $2W_{x'}(\alpha_d)$ instead of $W_{y'}(\alpha_d)$ is clear from the photo embedded in Fig. 8: there is not a standardized technique to determine the $y' = 0$ line, in other words, to locate the center of the "initial curve".

The results of the previous procedure for the determination of the contact angle 2ψ corresponding to contact length 2ℓ (Fig. 1b) are plotted in Fig. 8
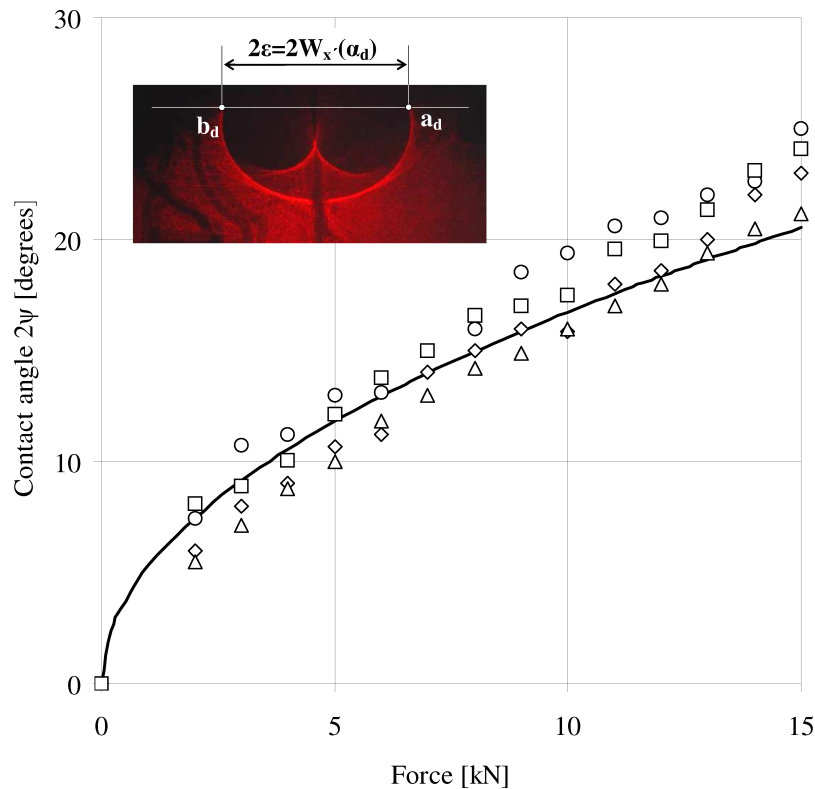

FIG. 8. Characteristic experimental (empty symbols) vs. analytic results (continuous line) for the contact length (each type of empty symbol corresponds to a single test). In the embedded figure the measure of the caustic's "characteristic dimension" required for determining the contact length is shown.

together with the theoretical predictions according to the present analysis (Subsection 2.1). It is concluded from Fig. 8 that for relatively low load levels (below 10 kN) the theoretical predictions are in very good agreement with the experimental results. For higher loads, the agreement is not satisfactory and the experimental data start exceeding systematically those of the theoretical analysis. This deviation is attributed to the gradual deviation of the material from its linear behavior; although, the stress at the disc's center is well below the linearity limit. Indeed, the stress field components at the immediate vicinity of the contact length (the area from which caustics pump data) increase abruptly, independently from the load distribution considered (uniform or parabolic or sinusoidal [43]), exceeding obviously the linearity limit of PMMA.

4. Discussion

The determination of the contact arc's length developed during the standardized execution of the Brazilian disc test is not a trivial experimental project. The techniques proposed are neither practical nor very accurate. For example, interposing a carbon paper between the disc and the jaw provides a rough estimation of the final length of the contact arc after the completion of the test. Nevertheless, the contact arc is gradually developed from (almost) zero (point contact when the load is zero) to its final extent. On the other hand, traditional optical techniques, like for example photoelasticity, can only be applied for a class of materials with special stress-optical properties. Moreover, due to high stress gradients in the immediate vicinity of the contact length [4, 43], the density of fringes unavoidably reduces the accuracy of these techniques.

On the contrary, the method of caustics can be applied for almost all materials either transparent or opaque. This is true even for rock-like materials or concrete (the materials usually examined using the Brazilian disc test) assuming that one of their lateral surfaces is covered (or painted) by a suitable light reflecting "skin". Of course, it should be mentioned that in case of construction materials, which are stiffer from the material used in the present experimental protocol, the magnitude of light deviation (and therefore of the caustic) becomes smaller downgrading perhaps the accuracy of the method (although for such materials the gradients of the stress field components are expected to be higher counterbalancing things). Clearly this point should be further studied in conjunction perhaps to modified experimental set-ups that increase magnification. Moreover for construction materials it is expected that the correction introduced in Subsection 2.2.2 becomes smaller (or even insignificant) considering that the magnitude of the displacement field's components is now too small.

Finally, the simplicity of the experimental set-up and also of the patterns obtained on the screen makes the method of reflected caustics a unique tool for exploring contact problems in general and the Brazilian disc test in particular. Moreover, the method of caustics is very sensitive to even the slightest variations of the contact arc. This is extremely important taking into account that, especially for brittle materials, the contact arc is very small. For example in case of a marble disc of diameter $D = 100$ mm the contact length just before fracture is estimated to about only 3.7 mm [43].

The demand for increased sensitivity and accuracy (recall that the majority of materials tested using the Brazilian disc test are of brittle nature and inevitably the contact arc is always very small) was the main reason for introducing here an improved version of the caustics method, the equations of which are derived with respect to the deformed disc's configuration.

Applying the reflected caustics method permits determination of the contact length during the experimental procedure without any intervention at the disc-jaw interface. Such an intervention may drastically influence the local stress field since interposing any material alters the boundary conditions by changing the coefficient of friction. In addition, knowledge of the contact length as a function of the external load permits determination of the actual profile of the radial pressure exerted by the jaw on the disc relieving the analysis from an additional arbitrary hypothesis concerning the load distribution.

Another advantage of the method is that it permits detection of the existence of shear stresses along the contact length. Indeed, as it is proved by THEOCARIS [36], the elevations of the two end-points a_d and b_d of the caustic curve must be equal to each other and their value must be given through Eq. (2.31). If this condition were not satisfied, shear stresses would have been developed violating the initial conditions considered.

The last point that should be carefully addressed is the dependence of the shape of the caustic on the extent of the contact arc or, in other words, on the external load. To highlight this point, the "initial curves" and the respective caustics are plotted in Fig. 9 for various load levels equal to 5, 15 and 40 kN. The figure was drawn for the material and set-up characteristics described in Subsection 2.2.2. It is seen from this figure that as the load increases the "initial curve" is transformed from a convex curve to a non-convex one. If the load is increased further the central point G of the "initial curve" will coincide with the origin of the reference system. This is the terminal value of load for which the critical condition $2|C^*| \geq \ell$ required for the existence of real roots of Eq. (2.24) is valid. From this point on, complex roots are obtained and the single "initial curve" splits into two independent loci. Concerning the caustic curves as the load increases they are gradually depressed until the "initial curve" ceases being a unique curve. The analysis of such caustics, i.e., in case the condition $2|C^*| < \ell$
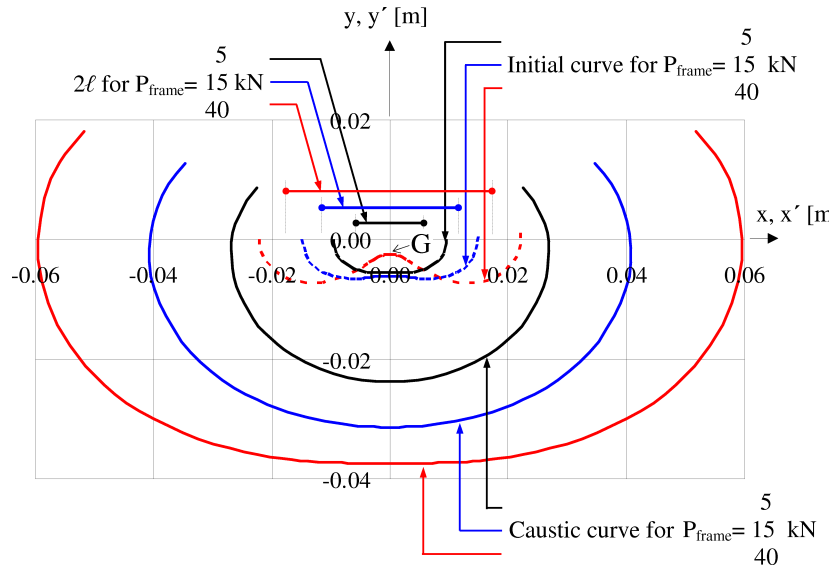
Fig. 9. The influence of the load level on the shape of the "initial curve" and the caustic.

is fulfilled, and the relation of their shape with the contact length are well beyond the scope of the present paper.

5. Conclusions

The contact length, 2ℓ at the disc-jaw interface in a standardized Brazilian disc test was determined both analytically and experimentally. From the analytic point of view 2ℓ was calculated according to a recently introduced method based on complex analysis [6]. For the experimental estimation of 2ℓ the method of reflected caustics was employed (properly adapted for the specific problem), mainly due to its increased accuracy and also due to its simple and easy-to-use experimental equipment. The accuracy of the method was improved by considering the actual shape of the corresponding "initial curve".

The agreement between theory and experiment is quite satisfactory for low load levels. As the load increases the experimentally obtained values for the contact length exceed those obtained analytically. Indeed, while for $P_{\mathrm{frame}} = 5$ kN the difference between theory and experiment is almost negligible (less than 3%) for $P_{\mathrm{frame}} = 15$ kN the deviation exceeds 15%. This is obviously due to the non-linear behavior of the material at the immediate vicinity of the contact arc since the local stress field is strongly amplified [43] even when the respective equivalent stress at the disc's center is below the critical value according to any failure criterion. The results of the present analysis can potentially advance a confusing point concerning the analysis of results obtained from the Brazilian disc test.

Indeed, with the aid of a preliminary test one can determine the $\ell = \ell(P_{\text{frame}})$ function. Then, employing the second of Eqs. (2.16) one obtains the variation of radial pressure $P(\tau)$ along the contact arc and moreover the actual stress field in the immediate vicinity of the disc-jaw interface. Nevertheless, it could be argued that such a complicated procedure is not worth the money. Such an aphorism could be acceptable as long as one considers only the stress field at the disc's center. However, it is known that for specific combinations of the disc's and jaw's stiffness fracture may originate far from the disc's center, in fact very close to the end points of the contact arcs [44] thus rendering knowledge of 2ℓ indispensable.

Before concluding it should be mentioned that reflected caustics are applicable only in case the lateral surface of the disc is seriously deformed. In the present study, plane stress conditions were assumed. The respective problem, i.e., the relation between the caustic and the contact length for plane strain conditions, is far more difficult. Perhaps in such a case solution could be given by employing the transmitted caustics method. However, transmission caustics presuppose transparent materials, which unfortunately is not the case of rock-like materials or concrete usually studied by the Brazilian disc test. In any case the specific problem should be studied further.

Acknowledgements

References

1. G. Hondros, *The evaluation of Poisson's ratio and the modulus of materials of a low tensile resistance by the Brazilian (indirect tensile) test with particular reference to concrete*, Aust. J. Appl. Sci., **10**, 243–268, 1959.

2. M. Mellor, I. Hawkes, *Measurement of tensile strength by diametral compression of discs and annuli*, Engineering Geology **5**, 173–225, 1971.

3. S.P. Timoshenko, J.N. Goodier, *Theory of Elasticity*, 3rd edition, McGraw-Hill, New York 1970.

4. Ch.F. Markides, D.N. Pazis, S.K. Kourkoulis, *Closed full-field solutions for stresses and displacements in the Brazilian disc under distributed radial load*, Int. J. Rock Mech. Min. Sci., **47**, 227–237, 2010.

5. F. Lanaro, T. Sato, O. Stephensson, *Microcrack modelling of Brazilian tensile tests with the boundary element method*, Int. J. Rock Mech. Min. Sci., **46**, 450–461, 2009.

6. S.K. Kourkoulis, Ch.F. Markides, P.E. Chatzistergos, *The standardized Brazilian disc test as a contact problem*, Int. J. Rock Mech. Min. Sci., **57**, 132–141, 2012.

7. S.K. Kourkoulis, Ch.F. Markides, P.E. Chatzistergos, *The Brazilian disc under parabolically varying load: Theoretical and experimental study of the displacement field*, Int. J. Solids and Structures, **49**, 959–972, 2012.

8. P. Manogg, *Anwendung der Schattenoptik zur Untersuchung des Zerreissvongangs von Platten*, Dissertation, Freiburg, Germany, 1964.

9. P. Manogg, *Schattenoptische Messung der spezifischen Bruchenergie waehrend des Bruchvorgangs bei Plexiglas*, in: Proceedings of the International Conference on Physics of Noncrystalline Solids, J.A. Prins [ed.], Delft, The Netherlands, 481–490, 1964.

10. P. Manogg, *Investigation of the rupture of a plexiglas plate by means of an optical method involving hoigh speed filming of the shadows originating around holes drilled in the plate*, Int. J. Fracture, **2**, 604–613, 1966.

11. P. Manogg, *Die Lichtablenkung durch eine elastisch beanspruchte Platte und die Schattenfiguren yon Kreis- und Risskerbe*, Glastechnische Berichte **39**, 323–329, 1966.

12. P.S. Theocaris, *Local yielding around a crack tip in plexiglas*, J. Applied Mechanics, **37**, 409–415, 1970.

13. P.S. Theocaris, E.E. Gdoutos, *An optical method for determining opening-mode and edge sliding-mode stress intensity factors*, J. Applied Mechanics **39**, 91–97, 1972.

14. J.F. Kalthoff, S. Winkler, J. Beinert, *Dynamic stress intensity factors for arresting cracks in DCB specimens*, Int. J. Fracture **12**, 317–319, 1976.

15. P.S. Theocaris, *Elastic Stress Intensity Factors Evaluated by Caustics*, in: Mechanics of Fracture, Vol. 7, Chapter 3, G.C. Sih [ed.], Sijthoff and Noordhoff, Amsterdam, The Netherlands, 1981.

16. G.A. Papadopoulos, *New formula of experimental stress intensity factor evaluation by caustics*, Int. J. Fracture, **171**, 79–84, 2011.

17. P.S. Theocaris, N.P. Andrianopoulos, *Dynamic three-point bending of short beams studied by caustics*, Int. J. Solids and Structures, **17**, 707–715, 1981.

18. G.A. Papadopoulos, *Dynamics caustics and its applications*, Optics and Lasers in Engineering, **13**, 211–249, 1990.

19. H.G. Georgiadis, G.A. Papadopoulos, *On the method of dynamic caustics in crack propagation experiments*, Int. J. Fracture, **54**, R19–R22, 1992.

20. X. Chunyang, Y. Xuefeng, F. Jing, *A study of dynamic caustics around running interface crack tip*, Acta Mechanica Sinica, **15**, 182–192, 1999.

21. Y. Xuefeng, X. Wei, J.G. Chang, Y.H. Yang, *Low velocity impact study of laminate composites with Mode I crack using dynamic optical caustics*, J. Reinforced Plastics and Composites, **23**, 1833–1844, 2004.

22. Y. Xuefeng, Z.H. Ping, Y. Hsien-Yang, *Dynamic caustic analysis of propagating Mode II cracks in transversely isotropic material*, J. Reinforced Plastics and Composites, **24**, 657–667, 2005.

23. Y. Xuefeng, X. Wei, *Recent application of caustics on experimental dynamic fracture studies*, Fatigue & Fracture of Engineering Materials & Structures, **34**, 448–459, 2011.

24. A.J. Rosakis, L.B. Freund, *Optical measurements of the plastic strain concentration at a tip in a ductile steel plate*, J. Engineering Materials Technology, **104**, 115–125, 1982.

25. M. Kikuchi, S. Hamanaka, *Evaluation of the J-Integral by the caustics method*, Transactions of the Japan Society of Mechanical Engineers A, **56** (532), 2581–2587, 1990.

26. N.T. Younis, L.W. Zachary, *A new technique for the determination of stress-optical constants using the shadow spot method*, Experimental Mechanics, **29**, 75–79, 1989.

27. P.S. Theocaris, D.N. Pazis, *Some further properties of caustics useful in mechanical applications*, Applied Optics, **20**, 4009–4018, 1981.

28. G.A. Papadopoulos, D.N. Pazis, *The non-linear solution of the mixed-mode caustics in birefringent materials*, Int. J. Fracture, **119**, L35–L40, 2003.

29. K. Gong, Z. Li, *Caustics method in dynamic fracture problem of orthotropic materials*, Optics and Lasers in Engineering, **46**, 614–619, 2008.

30. H.P. Rossmanith, R.E. Knasmillner, D. Semenski, *Crack-tip caustics in mechanically anisotropic materials*, Experimental Mechanics, **35**, 31–35, 1995.

31. D. Semenski, *Method of caustics in fracture mechanics of mechanically anisotropic materials*, Engineering Fracture Mechanics, **58**, 1–10, 1997.

32. D. Semenski, S. Jecić, *Experimental caustics analysis in fracture mechanics of anisotropic materials*, Experimental Mechanics, **39**, 177–183, 1999.

33. R. Yang, Z. Yue, Z. Sun, T. Xiao, D. Guo, *Dynamic fracture behavior of rock under impact load using the caustics method*, Mining Science and Technology, **19**, 79–83, 2009.

34. Y. Xuefeng, X. Wei, B. Shulin, Y. Hsien-Yang, *Caustics analysis of the crack initiation and propagation of graded materials*, Composites Science and Technology, **68**, 953–962, 2008.

35. N.T. Younis, *Designing an optical mechanics experiment,* World Transactions on Engineering and Technology Education, **9**, 137–144, 2011.

36. P.S. Theocaris, *The load distribution in the generalized contact problem by caustics*, in: Proceedings of the 3r^{d}National Congress on Theoretical and Applied Mechanics, Varna, Bulgaria, 13–16 September 1977, Vol. **III**, 105–143, 1978.

37. P. S. Theocaris, *Experimental study of plane elastic contact problems by the pseudo-caustics method*, J. Mechanics and Physics of Solids, **27**, 15–32, 1979.

38. D. Semenski, *Optical method of caustics – Fulfilled experimental application to the contact problem*, in: Proceedings of the XVII IMEKO World Congress Metrology in the 3rd Millennium, Dubrovnik, Croatia, June 22–27, 2003, 1952–1955, 2003.

39. K. Raptis, G.A. Papadopoulos, T.N. Costopoulos, A.D. Tsolakis, *Experimental study of load sharing in roller bearing contact by caustics and photoelasticity*, American J. Engineering and Applied Sciences, **4**, 294–300, 2011.

40. N.I. Muskhelishvili, *Some Basic Problems of the Mathematical Theory of Elasticity*, Noordhoff, Groningen, The Netherlands, 1963.

41. I. R. Wallhead, S. Güngör, L. Edwards, *Optimization of the optical method of caustics for the determination of stress intensity factors*, Opt. Laser Eng., **20**, 109–133, 1994.

42. D.N. Pazis, Z. Agioutantis, S.K. Kourkoulis, *The optical method of reflected caustics applied for a plate with a central hole: critical points and limitations*, Strain, **47**, 6, 489–498, 2011.

43. Ch.F. Markides, S.K. Kourkoulis, *The stress field in a standardized Brazilian disc: the influence of the loading type acting on the actual contact length*, Rock Mechanics and Rock Engineering, **45**, 145–158, 2012.

44. L. Diyuan, L.N.Y. Wong, *The Brazilian disc test for rock mechanics applications: Review and new insights*, Rock Mechanics and Rock Engineering, **46**, 269–287, 2013.